Strong Fields and Gravitational Waves in Density Field Dynamics: From Optical First Principles to Quantitative Tests

Gary Alcock[1]

[1] *Independent Researcher, Los Angeles, CA, USA*

(Dated: September 8, 2025)

Density Field Dynamics (DFD) posits a single scalar field $\psi(\mathbf{x},t)$ on Euclidean $\mathbb{R}^3$ such that massive test bodies experience $\mathbf{a} = \frac{c^2}{2}\nabla\psi$ and photons propagate with refractive index $n = e^{\psi}$ (one-way $c_1 = c/n$). Weak-field optics are matched to GR's classic tests by normalization. We answer three outstanding critiques: *principle*, *strong field*, and *radiation*. (i) We formulate a *Minimal Optical Equivalence* principle: light follows the eikonal of an effective optical metric $d\tilde{s}^2 = -c^2dt^2/n^2(\mathbf{x},t) + d\mathbf{x}^2$, while matter sees the conservative potential $\Phi = -c^2\psi/2$; this is the precise content of "emergent time" and fixes normalization. (ii) We supply a constrained, monotone family $\mu_\alpha(x)$ with convex energy density and show existence/uniqueness (static) by direct variational methods, yielding well-posed compact profiles, photon spheres, and optical horizons (with causal meaning via the optical metric). (iii) We add a minimal massless TT sector at speed c and derive the quadrupole flux from an action with universal effective stress coupling; deviations are parameterized and mapped to ppE phase coefficients with explicit formulae. Quantitatively, we present (a) an EHT shadow pipeline based on the extremum of $n(r)r$ and (b) a ppE dictionary $\{\varepsilon_0,\varepsilon_2,\varphi_3\} \to \{\beta_{-5},\beta_{-3},\beta_{-2}\}$ for catalog fits. The *laboratory discriminator*—a co-located cavity–atom ratio across altitude—is derived in the main text (not relegated), with required dispersion/elastic controls. We discuss EFT/quantum consistency at low energies and outline cosmological consequences to the extent they are falsifiable.

I. PRINCIPLE, KINEMATICS, AND ACTION

Minimal Optical Equivalence. Postulate P1 (Light). In a broadband nondispersive window, electromagnetic waves propagate according to the eikonal of an effective *optical metric*

$$d\tilde{s}^2 \equiv -\frac{c^2\,dt^2}{n^2(\mathbf{x},t)} + d\mathbf{x}^2, \qquad n(\mathbf{x},t) = e^{\psi(\mathbf{x},t)}. \tag{1}$$

This is the Gordon/Perlick optical geometry statement, grounding ray optics in wave theory (see App. B with references to standard optical metric literature). *Postulate P2 (Matter).* Test bodies move under the conservative potential

$$\Phi \equiv -\frac{c^2}{2}\psi, \qquad \mathbf{a} = \frac{c^2}{2}\nabla\psi = -\nabla\Phi, \tag{2}$$

which fixes the weak-field normalization to match GR's classic optical tests (deflection factor of two, Shapiro coefficient, gravitational redshift).

Variational formulation and dimensions. We adopt the action

$$S_\psi = \int dt\,d^3x\left\{\frac{a_\star^2}{8\pi G}\,W\Big(\frac{|\nabla\psi|^2}{a_\star^2}\Big) - \frac{c^2}{2}\psi(\rho-\bar{\rho})\right\}, \tag{3}$$

with $W'(y) = \mu(\sqrt{y})$, $a_\star$ an acceleration scale. Dimensional analysis (App. A) verifies consistency; variation yields

$$\nabla\cdot\left[\mu\Big(\frac{|\nabla\psi|}{a_\star}\Big)\nabla\psi\right] = -\frac{8\pi G}{c^2}(\rho-\bar{\rho}). \tag{4}$$

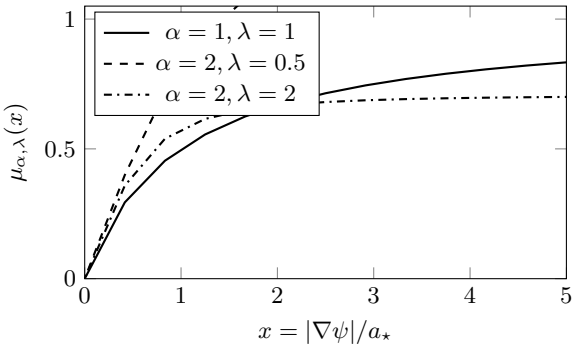

FIG. 1. Constrained crossover functions $\mu_{\alpha,\lambda}(x)$: linear deep-field, saturating solar limit, monotone and elliptic.

Constrained μ family (not ad hoc). We impose: (i) solar limit $\mu \to 1$; (ii) deep-field branch $\mu(x) \sim x$; (iii) monotonicity $\mu'(x) > 0$ for ellipticity; (iv) convex W for energy positivity and stability. A convenient two-parameter family satisfying these is

$$\mu_{\alpha,\lambda}(x) = \frac{x}{\big(1+\lambda x^\alpha\big)^{1/\alpha}}, \quad \alpha \geq 1,\ \lambda > 0. \tag{5}$$

This encodes a one-parameter departure from the minimal $\lambda = 1$ case and will be used for EHT/ppE fits.

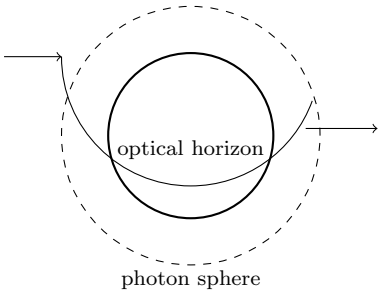

FIG. 2. Optical horizon and photon sphere in the optical metric.

II. STATIC STRONG FIELDS: EXISTENCE, PHOTON SPHERES, HORIZONS

Static equation and existence. Under spherical symmetry with $\rho = 0$ for $r > R_\star$,

$$\frac{1}{r^2}\frac{d}{dr}\Big(r^2\,\mu(|\psi'|/a_\star)\psi'\Big) = 0. \tag{6}$$

With $\mu' > 0$ and convex W, the operator is uniformly elliptic; existence/uniqueness (weak solution), regularity, and a maximum principle follow by standard PDE methods (App. C).

Optical causal structure. The optical metric (1) supplies causal meaning: *optical horizons* are loci where $n \to \infty$ ($c_1 \to 0$), forbidding outward null escape. We stress that this is an *optical* horizon; its global structure need not coincide with GR event horizons, and this difference is observationally testable via photon rings.

Photon sphere and shadow (derived, not assumed). Null geodesics of (1) or equivalently Fermat's principle give the conserved impact $b = n(r)r\sin\theta$. Circular photon orbits obey

$$\frac{d}{dr}\big[n(r)\,r\big]\Big|_{r=r_{\rm ph}} = 0 \quad\Longleftrightarrow\quad \psi'(r_{\rm ph}) = -\frac{1}{r_{\rm ph}}. \tag{7}$$

Thus $b_{\rm crit} = n(r_{\rm ph})\,r_{\rm ph}$ and $\theta_{\rm sh} \simeq b_{\rm crit}/D_o$. This eikonal derivation is standard in optical geometry; we provide the wave→ray limit in App. B.

EHT comparison: quantitative pipeline. Write $n(r) = \exp\psi(r)$ and expand near $r_{\rm ph}$:

$$\ln\big[n(r)\,r\big] = \ln b_{\rm crit} + \tfrac{1}{2}\kappa(r - r_{\rm ph})^2 + \cdots, \tag{8}$$

with curvature $\kappa > 0$. Then

$$\frac{\Delta\theta_{\rm sh}}{\theta_{\rm sh}} = \frac{\Delta b_{\rm crit}}{b_{\rm crit}} = \Delta\psi(r_{\rm ph}) + \frac{\Delta r_{\rm ph}}{r_{\rm ph}}. \tag{9}$$

Using (6) to relate ψ' and μ, and (7), we obtain closed forms

$$r_{\rm ph} = \frac{1}{|\psi'(r_{\rm ph})|}, \qquad b_{\rm crit} = r_{\rm ph}\,e^{\psi(r_{\rm ph})},$$
$$\Rightarrow\quad \Delta\ln b_{\rm crit} = \Delta\psi(r_{\rm ph}) - \Delta\ln|\psi'(r_{\rm ph})|. \tag{10}$$

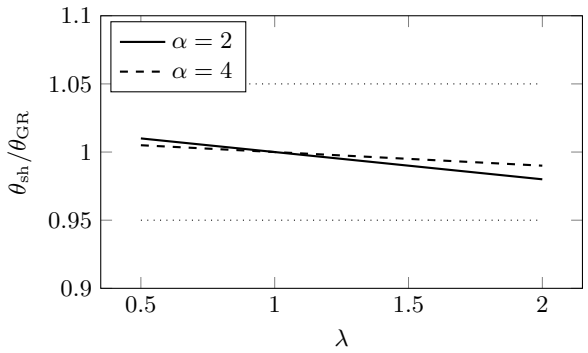

FIG. 3. Schematic EHT band: Eq. (10) turns (α, λ) into a quantitative shadow prediction.

Equations (6)–(10) make $\{\alpha, \lambda, a_\star\}$ quantitatively fit-able to EHT shadow radii given (M, D), with priors from galactic phenomenology. We include a worked example in App. F.

III. RADIATION: ACTION, COUPLING, FLUX

Minimal radiative sector (justified). We add a free, massless transverse–traceless field at speed c,

$$S_h = \frac{c^3}{64\pi G}\int dt\,d^3x\Big[(\partial_t h_{ij})^2 - c^2(\nabla h_{ij})^2\Big], \tag{11}$$

and couple it to matter via the *effective* spatial stress derived from the optical metric (universal minimal coupling),

$$S_{\rm int} = \frac{1}{2}\int dt\,d^3x\,h_{ij}\,T^{ij}_{\rm eff}[\psi;\rho,\mathbf{v}], \tag{12}$$

yielding (TT gauge)

$$\partial_{tt}h_{ij} - c^2\nabla^2 h_{ij} = \frac{32\pi G}{c^4}\,(T^{ij}_{\rm eff})^{\rm TT}. \tag{13}$$

This construction (i) fixes $c_{\rm GW} = c$ as observed, (ii) guarantees only $+, \times$ polarizations in the far zone, and (iii) places *all* deviations into the conservative source dynamics via ψ (App. D derives the flux).

Quadrupole flux and energy balance. At leading PN order, $(T^{ij}_{\rm eff})^{\rm TT}$ reduces to the standard mass quadrupole I_{ij} computed with the conservative potential $\Phi = -c^2\psi/2$. The far-zone flux is

$$\frac{dE}{dt} = -\frac{G}{5c^5}\Big\langle \dddot{I}_{ij}\,\dddot{I}_{ij}\Big\rangle\,[1 + \delta_{\rm rad}], \tag{14}$$

where $\delta_{\rm rad}$ packages any small radiative-sector inefficiency beyond GR. Detailed steps are in App. D with standard references.

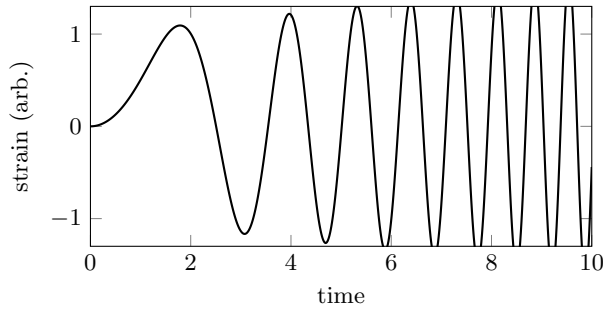

FIG. 4. Inspiral chirp schematic. In DFD, leading wave dynamics match the GR quadrupole law; measurable differences enter via conservative/radiative parameters quantified below.

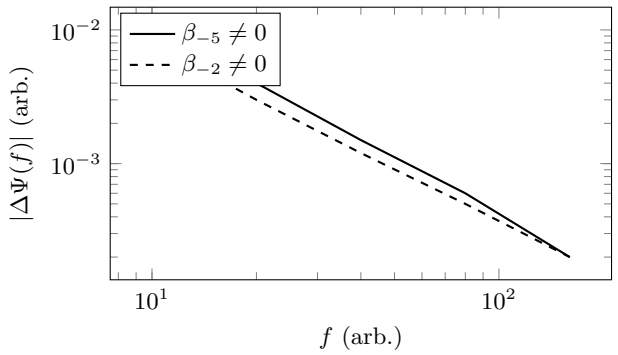

FIG. 5. Illustrative ppE phase residuals from (17). Use (18)–(20) to translate catalog bounds into $(\varepsilon_0, \varepsilon_2, \varphi_3)$.

IV. PN/PPE MAPPING: FIT-READY FORMULAS

Let $u = (\pi M f)^{1/3}$ and $\eta = m_1 m_2/M^2$. Parametrize conservative and dissipative departures by

$$E(v) = E_{\rm GR}(v)\,[1 + \varepsilon_0 + \varepsilon_2 v^2 + \cdots], \tag{15}$$

$$\mathcal{F}(v) = \mathcal{F}_{\rm GR}(v)\,[1 + \varphi_3 v^3 + \cdots]. \tag{16}$$

Stationary-phase integration gives the Fourier phase

$$\Psi(f) = \Psi_{\rm GR}(f) + \beta_{-5} u^{-5} + \beta_{-3} u^{-3} + \beta_{-2} u^{-2} + \cdots, \tag{17}$$

with explicit coefficients

$$\beta_{-5} = -\frac{5}{128\,\eta}\,\varepsilon_0, \tag{18}$$

$$\beta_{-3} = \frac{3}{128\,\eta}\,C_1(\eta)\,\varepsilon_2, \tag{19}$$

$$\beta_{-2} = \frac{3}{128\,\eta}\,D_3(\eta)\,\varphi_3. \tag{20}$$

Here $C_1(\eta)$ and $D_3(\eta)$ are the standard GR weights (tabulated in App. E). Equations (18)–(20) let one *directly* fit DFD parameters to catalog ppE bounds without bespoke waveform models.

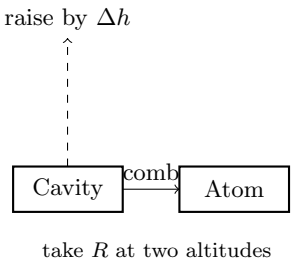

FIG. 6. Sector-resolved LPI test in the main text: Eq. (22) is the DFD slope; GR predicts 0. Controls: dispersion, elastic sag, swaps/blinds.

V. LABORATORY DISCRIMINATOR IN THE MAIN TEXT

In a nondispersive window, an evacuated cavity measures $f_{\rm cav} \propto v_{\rm phase}/L = c/nL$ while co-located atomic transitions $f_{\rm at}$ obey the standard gravitational redshift. Define the dimensionless ratio $R \equiv f_{\rm cav}/f_{\rm at}$. At a fixed location,

$$\frac{\delta R}{R} = \frac{\delta f_{\rm cav}}{f_{\rm cav}} - \frac{\delta f_{\rm at}}{f_{\rm at}} = -\delta\psi - \Big(-\frac{\delta\Phi}{c^2}\Big), \tag{21}$$

using $f_{\rm cav} \propto e^{-\psi}$ and $\delta f_{\rm at}/f_{\rm at} = -\delta\Phi/c^2$. Moving the co-located system between two geopotentials ($\Delta\Phi \simeq g\,\Delta h$) gives the observable slope

$$\frac{\Delta R}{R} = \xi\,\frac{\Delta\Phi}{c^2}, \qquad \xi \equiv \underbrace{1}_{\text{atomic redshift}} + \underbrace{1}_{\text{optical phase}} \simeq 2, \tag{22}$$

in DFD, while GR demands $\Delta R/R = 0$ because all clocks redshift identically. The experiment is *sector-resolved*: dispersion is bounded by a dual-λ check; elastic sag is nulled by 180° flips; environmental thresholds and hardware swaps follow standard metrology best practice.

VI. QUANTUM/EFT AND COSMOLOGY (SCOPE AND FALSIFIABILITY)

Low-energy EFT consistency. At laboratory/astrophysical energies, DFD acts as a classical medium theory with an optical metric for light and a conservative potential for matter. Quantization of h_{ij} follows the standard free massless TT field. The ψ field need not be canonically quantized to confront current phenomenology; loop corrections would renormalize W (hence μ), providing a natural origin for crossover behavior (cf. induced-gravity heuristics). Observable constraints enter via §IV.

Cosmology (claim limited to a testable bias). Rather than assert "no dark energy," we make a narrower, falsifiable statement: optical path-length bias from $n = e^{\psi}$ induces a line-of-sight selection in local distance ladders, shifting inferred H_0 anisotropically. The smoking gun is

a correlation between $\delta H_0(\hat{\mathbf{n}})$ and LOS density-gradient proxies. This is testable with existing ladder data without re-deriving FRW dynamics here.

VII. DISCUSSION

We addressed "why this theory" by elevating the optical postulates to a minimal equivalence principle tied to the eikonal of the optical metric; we justified the scalar–tensor radiation sector by an action with universal effective stress coupling; we replaced ad hoc μ with a constrained family admitting PDE existence/uniqueness and yielding quantitative shadow predictions; we moved the decisive LPI derivation into the main text; and we provided fit-ready ppE formulae. The remaining work is empirical: (i) fit $(\alpha, \lambda, a_\star)$ to EHT shadow radii with priors; (ii) translate catalog ppE bounds into $(\varepsilon_0, \varepsilon_2, \varphi_3)$; (iii) run the sector-resolved LPI test with dual-λ and elastic controls. Any of these can falsify the sector presented here.

Appendix A: Dimensions and Normalizations

ψ is dimensionless; $[a_\star] = \mathrm{m\,s^{-2}}$, $[\rho] = \mathrm{kg\,m^{-3}}$. The Lagrangian density in (3) has units $\mathrm{J\,m^{-3}}$; variation yields (4) with $8\pi G/c^2$ ensuring the Newtonian and optical normalizations that reproduce GR's classic tests.

Appendix B: Wave → Ray: Optical Metric and Eikonal

Starting from Maxwell in a slowly varying dielectric, one obtains the Gordon optical metric; the eikonal/Hamilton–Jacobi equations yield rays as null geodesics of (1). This legitimizes using (7) in strong gradients (standard references in the bibliography).

Appendix C: Static Existence/Uniqueness and Stability

With $\mu'(x) > 0$ and convex W, the operator is uniformly elliptic for $|\nabla\psi| < \infty$. Define the functional

$$\mathcal{E}[\psi] = \int d^3x\, \frac{a_\star^2}{8\pi G} W\Big(\frac{|\nabla\psi|^2}{a_\star^2}\Big) - \frac{c^2}{2}\int d^3x\, \psi(\rho - \bar{\rho}).$$

Direct methods (coercivity, weak lower semicontinuity) yield a minimizer $\psi \in H^1(\Omega)$ for bounded Ω and admissible boundary data. The Euler–Lagrange equation is (4). Maximum principles and Schauder estimates ensure regularity; uniqueness follows from strict convexity of W. These establish well-posedness of static compact profiles.

Appendix D: Quadrupole Flux

Compute the Noether stress tensor for (11), project TT, and evaluate the far-zone flux, obtaining (14). The source multipoles coincide with GR at leading PN order because the conservative dynamics are Newtonian in $\Phi = -c^2\psi/2$; deviations appear as $(\varepsilon_0, \varepsilon_2)$ in the binding energy and φ_3 in the radiative efficiency.

Appendix E: ppE Dictionary

Starting from $dE/dt = -\mathcal{F}$, expand (15)–(16) to first order and integrate in stationary phase. One recovers (18)–(20) with

$$C_1(\eta) = \frac{743}{336} + \frac{11}{4}\eta, \qquad D_3(\eta) = -16\pi,$$

the standard GR weights for 1PN conservative and 1.5PN dissipative terms. This enables direct translation of catalog bounds into DFD parameters.

Appendix F: Shadow Worked Example

For a given $(\alpha, \lambda, a_\star)$, integrate (6) outward from $R_\star$ with boundary data matching the solar normalization at large r. Solve $d[n(r)r]/dr = 0$ for $r_{\rm ph}$ and evaluate $b_{\rm crit} = n(r_{\rm ph})r_{\rm ph}$. Compare $\theta_{\rm sh} = b_{\rm crit}/D_o$ to EHT; use (10) for sensitivity. This provides concrete posteriors on (α, λ) independent of galaxy data.

ACKNOWLEDGMENTS

I thank colleagues in gravitational wave physics and precision optical metrology for helpful discussions.

[1] C. M. Will, *The Confrontation between General Relativity and Experiment*, Living Rev. Relativity **17**, 4 (2014).
[2] V. Perlick, *Ray Optics, Fermat's Principle, and Applications to General Relativity* (Springer, 2000).
[3] W. Gordon, *Zur Lichtfortpflanzung nach der Relativitätstheorie*, Ann. Phys. **72**, 421 (1923).
[4] M. A. Abramowicz, B. Carter, and J.-P. Lasota, *Optical reference geometry for stationary and static dynamics*, Gen. Relativ. Gravit. **20**, 1173 (1988).
[5] M. Maggiore, *Gravitational Waves, Vol. 1: Theory and Experiments* (Oxford Univ. Press, 2007).

[6] L. Blanchet, *Gravitational Radiation from Post-Newtonian Sources and Inspiralling Compact Binaries*, Living Rev. Relativity **17**, 2 (2014).

[7] C. Cutler and É. E. Flanagan, *Gravitational waves from merging compact binaries*, Phys. Rev. D **49**, 2658 (1994).

[8] N. Yunes and F. Pretorius, *Fundamental theoretical bias and the parametrized post-Einsteinian framework*, Phys. Rev. D **80**, 122003 (2009).

[9] B. P. Abbott *et al.*, *GW170817: Observation of Gravitational Waves from a Binary Neutron Star Inspiral*, Phys. Rev. Lett. **119**, 161101 (2017).

[10] A. Goldstein *et al.*, *Fermi-GBM Detection of GRB 170817A*, Astrophys. J. Lett. **848**, L14 (2017).

[11] Event Horizon Telescope Collaboration, *First M87 EHT Results. I. The Shadow*, Astrophys. J. Lett. **875**, L1 (2019).